Supplementary Material

Tao Liu, Jun Cheng, Shan Tan
Huazhong University of Science and Technology, Wuhan, China
shantan@hust.edu.cn

1. Additional Experiments for DDL

1.1. Computational cost

For a more fair comparison, we compare the EDSR and DDL-EDSR in terms of their computational costs. As shown in Tab. 1, the DDL method improves SR performance at the cost of slightly increased model parameters and FLOPs. To rigorously evaluate the DDL, we enrich the baseline EDSR model to a deeper version (denoted as EDSR†). It can be observed that our proposed DDL-EDSR still shows a remarkable performance gain compared with EDSR†, indicating the effectiveness of the proposed DDL method.

1.2. Ablation study of DDL-EDSR

We conduct an ablation study on the different components of the DDL method. We isolate the impact of the dual-domain model structure and the dual-domain loss. Results shown in Tab. 2 imply that the standalone use of either dual-domain structure or loss can benefit SR performance (respectively improve the PSNR metric by 0.318 dB and 0.053 dB). Together use of the dual-domain structure and loss (i.e. our full DDL method) can bring more PSNR gains (0.531 dB).

1.3. Extension to RCAN

To further demonstrate the effectiveness of the proposed DDL strategy, we implement DDL based on RCAN [7], and term the model as DDL-RCAN. The modifications on RCAN are two-fold: 1) All residual channel attention blocks (RCAB) are replaced by proposed DDL-RCAB. Similar to DDL-RB, DDL-RCAB adopts two parallel branches to extract informative features in the spatial and frequency domains, respectively. The output features of the two branches are fused and them modulated by another channel attention module. 2) As implemented in DDL-EDSR, two output heads are developed to reconstruct SR images and spectra simultaneously. We train DDL-RCAN under the same setting of RCAN for a fair comparison. The quantitative results on benchmarks are shown in Tab. 3. We can observe the remarkable and consistent performance improvement across scales and benchmarks is obtained when combining RCAN with the DDL method. This demonstrate the effectiveness and versatility of our proposed DDL. Any other CNN backbones for image SR can utilize it to boost model performance.

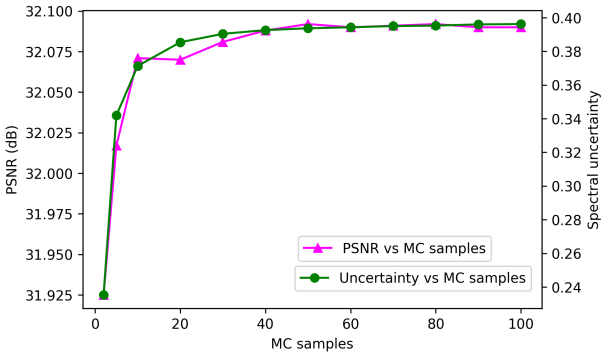

Figure 1. Reconstruction PSNR metrics and average spectral uncertainty with the increase of MC samples. The results are obatined on Set5 [1] for $\times 4$ SR.

2. Number of MC samples

In this work, we employ MC-dropout [3] to approximate Bayesian inference. MC samples are generated through multiple stochastic forward passes. Determining the number of MC samples is an important issue. Previous work [6] shows that more MC samples could yield better SR reconstruction as well as more accurate uncertainty estimate. Here we also investigate the effect of MC samples for SR performance and spectral uncertainty. As seen in Fig. 1, both reconstruction PSNR and spectral uncertainty increase with the increase of MC samples, and then converge to stable values. Consider the performance-efficiency trade-off, we choose 40 as the number of MC samples.

Table 1. Comparison of PSNR metric and computational cost for $\times 2$ SR. EDSR† denotes a deeper EDSR with 20 residual blocks.

model	Urban100	Manga109	Params (M)	FLOPs (G)
EDSR	31.881	38.362	1.37	90.0
EDSR†	32.018	38.471	1.66	109.3
DDL-EDSR	32.412	38.897	1.64	107.3

Table 2. Ablation study of DDL method on Urban100 at $\times 2$ scale.

Dual-domain structure	Dual-domain loss	PSNR↑	SSIM↓
		31.881	0.9263
✓		32.199	0.9288
	✓	31.934	0.9266
✓	✓	32.412	0.9308

Table 3. Quantitative evaluation of the proposed DDL method based on RCAN.

Model	Scale	Set5		Set14		B100		Urban100		Manga109	
		PSNR↑	SSIM↑	PSNR↑	SSIM↑	PSNR↑	SSIM↑	PSNR↑	SSIM↑	PSNR↑	SSIM↑
RCAN	$\times 2$	38.27	0.9614	34.12	0.9216	32.41	0.9021	33.34	0.9384	39.44	0.9786
DDL-RCAN		38.38	0.9617	34.27	0.9230	32.52	0.9025	33.65	0.9401	39.74	0.9792
RCAN	$\times 3$	34.74	0.9299	30.65	0.8482	29.32	0.8111	29.09	0.8702	34.44	0.9499
DDL-RCAN		34.96	0.9310	30.79	0.8499	29.41	0.8126	29.34	0.8754	34.72	0.9525
RCAN	$\times 4$	32.63	0.9002	28.87	0.7889	27.77	0.7436	26.82	0.8087	31.22	0.9173
DDL-RCAN		32.85	0.9021	28.99	0.7902	28.84	0.7444	26.96	0.8132	31.45	0.9194

3. Adversarial Attack

3.1. Projected Gradient Descent

So as to quantify spectral uncertainty under adversarial attacks, projected gradient descent (PGD) algorithm [4] is employed to generate adversarial LR images. The goal is to add a perturbation on input LR where the perturbation is visually imperceptible but could cause SR models produce unwanted artifacts. Formally, PGD is to solve the optimization problem:

$$\begin{aligned} &\arg\max_{\delta\in\Delta} \mathcal{L}(\boldsymbol{I}^{LR}, \delta), \\ &\mathcal{L}(\boldsymbol{I}^{LR}, \delta) = \|f(\boldsymbol{I}^{LR}) - f(\boldsymbol{I}^{LR} + \delta)\|_1 \end{aligned} \tag{1}$$

where $f(\cdot)$ is a well-trained SR model. δ is the perturbation on $\boldsymbol{I}^{LR}$. Δ denotes an allowable set of perturbations. PGD uses the infinite norm ball as the Δ:

$$\Delta = \{\delta : \|\delta\|_\infty < \kappa\}, \tag{2}$$

in which κ is a hyper-parameter of perturbation level. To solve the optimization problem, PGD follows the iterative update rule:

$$\begin{aligned} &\delta_{t+1} = \delta_t + \eta \cdot sign(\nabla_\delta \mathcal{L}(\boldsymbol{I}^{LR}, \delta)), \\ &\delta_{t+1} = min(max(\delta_{t+1}, -\kappa), \kappa), \end{aligned} \tag{3}$$

in which η is the step size of each update which is set to 1 in this work. After T iterations, adversarial LR images can be obtained by $\boldsymbol{I}^{LR} + \delta_T$.

3.2. Results under Adversarial Attacks

The quantitative results of image SR ($\times 4$) and the corresponding spectra uncertainty under adversarial attacks of diverse perturbation levels are exhibited in Tab. 4. One can observe that a very small perturbation ($\kappa = 1/255$) could result in severe performance drop. Bayesian model shows a better robustness against such adversarial attacks. With the increase of perturbation levels, the SR performance deteriorates more heavily. As for reconstruction uncertainty, spectral uncertainty increases with the increase of perturbation levels.

3.3. Partial Adversarial Attack

Instead of adding a perturbation on the whole region of the given LR image, partial adversarial attack aims to attack some specific parts [2]. Here we only exert perturbations on the left half of the given LR image, as displayed in Fig. 2. Even if the spectral uncertainty behaves more sensitive in detecting adversarial attacks, it seems to be incompetent in locating image regions which are under attacks since it captures reconstruction uncertainty in a global way. Therefore,

Table 4. The SR ($\times 4$) performance and spectral uncertainty under adversarial attacks.

Model	Attack level	PSNR	Spectral uncertainty
DDL-EDSR	0/255	30.10	/
Bayesian DDL-EDSR	0/255	29.97	0.3644
DDL-EDSR	1/255	24.43	/
Bayesian DDL-EDSR	1/255	26.57	0.4144
Bayesian DDL-EDSR	2/255	23.09	0.4533
Bayesian DDL-EDSR	3/255	20.79	0.4878

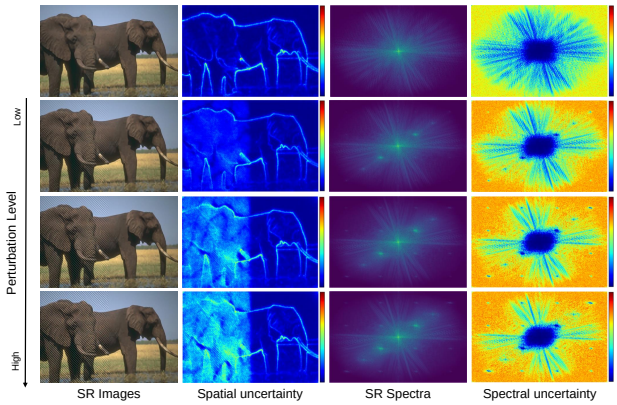

Figure 2. Dual-domain $\times 4$ SR results and corresponding uncertainty under partial adversarial attacks of different perturbation levels. From top to bottom: the perturbation level is 0/255 (without attack), 1/255, 2/255, 3/255. The example image is from B100 [5].

the proposed spectral uncertainty has pros and cons. Spatial pixel-wise and spectral frequency-wise uncertainty complement each other and can be employed jointly to quantify image SR uncertainty locally and globally.

References

[1] Marco Bevilacqua, Aline Roumy, Christine Guillemot, and Marie-Line Alberi-Morel. Low-complexity single-image super-resolution based on nonnegative neighbor embedding. In *BMVC*, 2012. 1

[2] Jun-Ho Choi, Huan Zhang, Jun-Hyuk Kim, Cho-Jui Hsieh, and Jong-Seok Lee. Evaluating robustness of deep image super-resolution against adversarial attacks. *2019 IEEE/CVF International Conference on Computer Vision (ICCV)*, pages 303–311, 2019. 2

[3] Yarin Gal and Zoubin Ghahramani. Dropout as a bayesian approximation: Representing model uncertainty in deep learning. *ArXiv*, abs/1506.02142, 2016. 1

[4] Aleksander Madry, Aleksandar Makelov, Ludwig Schmidt, Dimitris Tsipras, and Adrian Vladu. Towards deep learning models resistant to adversarial attacks. *ArXiv*, abs/1706.06083, 2018. 2

[5] David R. Martin, Charless C. Fowlkes, Doron Tal, and Jitendra Malik. A database of human segmented natural images and its application to evaluating segmentation algorithms and measuring ecological statistics. *Proceedings Eighth IEEE International Conference on Computer Vision. ICCV 2001*, 2:416–423 vol.2, 2001. 3

[6] Mattias Teye, Hossein Azizpour, and Kevin Smith. Bayesian uncertainty estimation for batch normalized deep networks. In *ICML*, 2018. 1

[7] Yulun Zhang, Kunpeng Li, Kai Li, Lichen Wang, Bineng Zhong, and Yun Raymond Fu. Image super-resolution using very deep residual channel attention networks. In *ECCV*, 2018. 1